

Damage Detection of a Building Caused by the 2011 Tohoku-Oki Earthquake with Seismic Interferometry

by Nori Nakata, Wataru Tanaka, and Yoshiya Oda

Abstract We apply seismic interferometry based on deconvolution to earthquake data observed in a building at Tokyo Metropolitan University to extract building response and estimate velocities and frequencies of traveling waves inside the building. The building is a 10-story reinforced concrete structure in Tokyo, Japan. The earthquake data were recorded 2 months before, 6 months after, and 16 months after the M_w 9.0 Tohoku-Oki earthquake (11 March 2011). The observation period of each acquisition was 20–30 days. We analyze more than 300 earthquakes recorded in these time periods, and we find significant reduction ($\sim 20\%$) in wave velocities and fundamental-mode frequencies after the Tohoku-Oki earthquake. Because deconvolution interferometry separates the response of the building from the effect of complicated wave propagation outside the building, we interpret that this reduction is mostly related to the building. We can also estimate frequencies of the fundamental mode from observed data, and these frequencies contain the responses of building and the ray paths from hypocenters. Therefore, as we find from the data, the frequencies estimated from observed data are generally lower than those from deconvolved waveforms due to the effects of wave propagation. Although the velocities in the building decrease $\sim 20\%$ after the Tohoku-Oki earthquake, we cannot find significant reduction in the S -wave velocities at the near surface (depth shallower than 100 m). This fact indicates the decrease in velocities is mainly related to the building, and hence, with deconvolution interferometry, we can detect damages to the building caused by the Tohoku-Oki earthquake.

Introduction

Seismic interferometry reconstructs wavefields propagating between receivers using the waves originally generated by, for example, earthquakes, traffic, and active sources (Claerbout, 1968; Wapenaar, 2004). From the reconstructed wavefields, one can characterize a medium along the wavepaths (Vasconcelos and Snieder, 2008; Prieto *et al.*, 2009; Ruigrok *et al.*, 2010; Nakata *et al.*, 2015). Seismic interferometry works well for 1D wave propagation (Miyazawa *et al.*, 2008; Pech *et al.*, 2012; Nakata, 2013) because all waves come from stationary points (Snieder, 2004b). For 2D or 3D problems, we can extend seismic interferometry based on multidimensional deconvolution (Wapenaar *et al.*, 2008; Nakata *et al.*, 2014).

With an assumption of 1D wave propagation, Snieder and Şafak (2006) applied seismic interferometry based on deconvolution to earthquake data observed in the Millikan Library at the California Institute of Technology for extracting building response. The assumption is satisfied at lower frequencies (i.e., longer wavelength). For the 1D case, seismic interferometry with deconvolution is similar to the computation of transfer functions. Todorovska (2009a) and Rahmani *et al.* (2015) suggested the response also depends on the foundation rocking when one considers models with higher degrees of free-

dom of the base of the building, such as horizontal and rocking motions, for which the response is coupled. The deconvolution technique is useful to extract and monitor building response, and widely applied to many buildings (Kohler *et al.*, 2007; Todorovska and Trifunac, 2008). In high-seismicity regions and/or for long-term observation, we can use this technique for time-lapse studies (Nakata *et al.*, 2013). Even if earthquakes occur at different locations, Nakata *et al.* (2013) could extract similar building response, which indicates the robustness of this technique. Also, we can apply seismic interferometry to ambient noise data observed in buildings (Prieto *et al.*, 2010; Nakata and Snieder, 2014), although amplitudes of wave propagation still need further studies.

Deconvolution interferometry changes the boundary condition at the base of the building when we deconvolve observed wavefields at each floor with waves recorded by the receiver at the base (Snieder *et al.*, 2006; Nakata *et al.*, 2013). Because of the modification of the boundary condition, the response obtained by deconvolution interferometry is related to that of the building itself assuming no rocking motion at the base. In contrast, we can estimate a response that mixes building response and wave propagation outside

the building from the observed data with, for example, mode analyses (Trifunac, 1972; Trifunac *et al.*, 2001). Therefore, by separately using observed and deconvolved wavefields, we can extract two different responses.

In this study, we analyze earthquake records observed inside a building at Tokyo Metropolitan University, Tokyo, Japan. We observed data in three time periods; one before the M_w 9.0 Tohoku-Oki earthquake (11 March 2011) and two after. The building is about 400 km away from the epicenter of the mainshock. First, we briefly review deconvolution interferometry and introduce our data. Then, we characterize the damage caused by the Tohoku-Oki earthquake with velocities and frequencies of traveling waves extracted by deconvolution interferometry. Finally, we discuss differences of responses obtained from observed and deconvolved data.

Deconvolution Interferometry

We use deconvolution interferometry with an assumption of vertical wave propagation (1D propagation) with constant wavenumber and attenuation of the building and without internal reflections to simplify equations. The assumption of constant wavenumber and attenuation along the height is weakened by using the WKBJ approximation (a linearized solution of a 1D wave equation) (Snieder, 2004a; Nakata *et al.*, 2013). Ebrahimian and Todorovska (2014, 2015) introduce bending deformation and frequency-dependent attenuation to the beam model to explain the dispersive response of observed deconvolved wavefields in buildings. Details of the techniques are summarized in Nakata *et al.* (2013) and Nakata and Snieder (2014), and here we briefly review this technique. With the assumption above, an earthquake record at height z can be written in the frequency domain as

$$u(z, \omega) = \frac{S(\omega)\{e^{ikz}e^{-\gamma|k|z} + e^{ik(2H-z)}e^{-\gamma|k|(2H-z)}\}}{1 - R(\omega)e^{2ikH}e^{-2\gamma|k|H}}, \quad (1)$$

in which $S(\omega)$ is the incoming waveform at the base of the building, $R(\omega)$ is the reflection coefficient due to the ground coupling, k is the wavenumber, γ is the attenuation coefficient, H is the height of the building, and i is the imaginary unit. Here, for convenience, we consider the ground level is at $z = 0$ and positive z for elevation. The waveform $S(\omega)$ contains a source wavelet of the earthquake and the effect of wave propagation beneath the building. Equation (1) indicates the waves are reverberating between the top and bottom of the building with energy loss caused by the intrinsic attenuation of the building (γ) and the boundary condition at the base ($R(\omega)$). When we deconvolve the observed waves at z with those at the base ($z = 0$), we obtain

$$\begin{aligned} D(z, 0, \omega) &= \frac{u(z, \omega)}{u(0, \omega)} \left(\frac{u(z, \omega)u^*(0, \omega)}{|u(0, \omega)|^2 + \epsilon} \right) \\ &= \frac{e^{ikz}e^{-\gamma|k|z} + e^{ik(2H-z)}e^{-\gamma|k|(2H-z)}}{1 + e^{2ikH}e^{-2\gamma|k|H}}, \quad (2) \end{aligned}$$

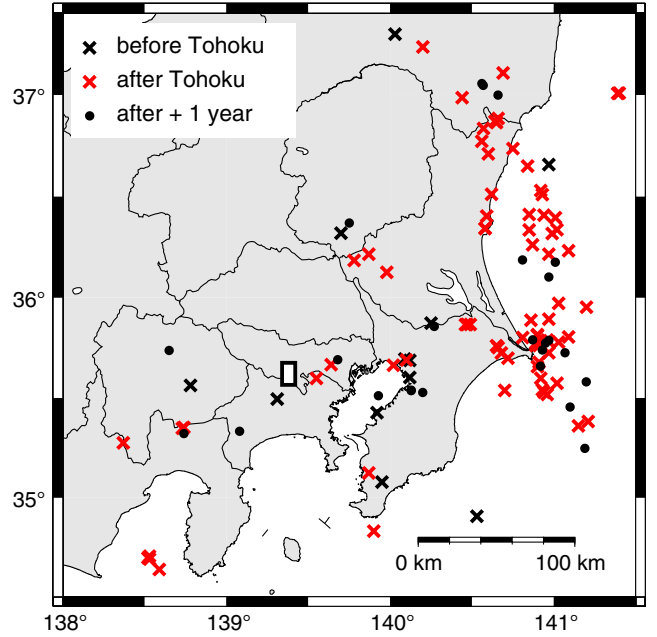


Figure 1. Locations of the building (rectangle, not to scale) and epicenters of earthquakes studied (dots and crosses) in three time periods. In each time period, we use the same symbol for both north–south and east–west components. The time periods and number of earthquakes are shown in Table 2. Only earthquakes listed in the earthquake catalog provided by the Japan Meteorological Agency (JMA) are shown on the map. The color version of this figure is available only in the electronic edition.

in which $*$ is the complex conjugate and ϵ is the regularization parameter for deconvolution. Here, ϵ is the 5% of average power spectra at each earthquake. One can also use spectral smoothing for regularization of equation 2 (Sawazaki *et al.*, 2009). We can choose any receivers for the denominator of the deconvolution, and each receiver represents different building response (Nakata *et al.*, 2013). Here, we compute the deconvolution with the bottom receiver. Apparently, equation (2) is not related to the incoming wavelets ($S(\omega)$) and the ground coupling ($R(\omega)$). By considering two or higher degrees of freedom of the foundation, the deconvolved wavefields are not perfectly independent from the effect of the foundation coupling (Todorovska, 2009a; Rahmani *et al.*, 2015). Note that based on the similarity between equations (1) and (2), deconvolved wavefields represent the same wave propagation as observed wavefields (equation 1) with simple incoming wavelets and boundary condition. Therefore, we can use the deconvolved waves for estimating velocities, frequencies of each mode, and attenuation of the building (Nakata *et al.*, 2013).

Building and Earthquake Records

Earthquake data are recorded inside Building 9 at the Minami-Osawa campus, Tokyo Metropolitan University, Tokyo, Japan (Fig. 1). The building is located ~ 400 km away from the epicenter of the Tohoku-Oki earthquake, and the maximum acceleration during the mainshock at the

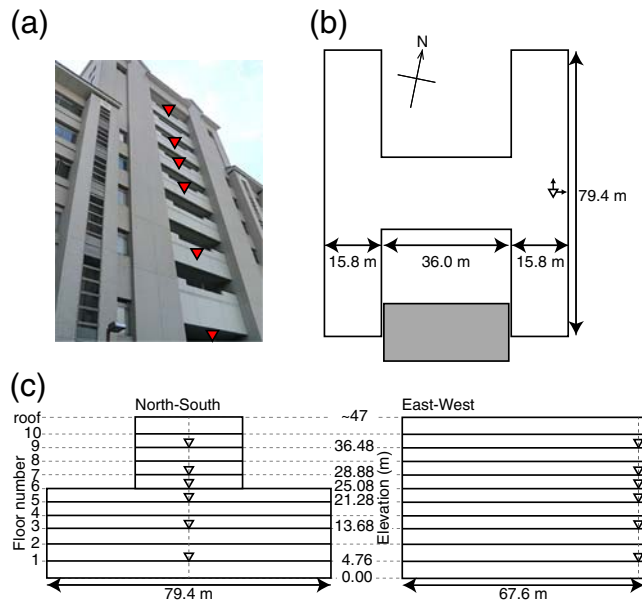


Figure 2. (a) East side of the building. Receivers are deployed at the east edge. (b) Plan view of the building. According to the shape of the building, we define the component parallel to the 79.4 m side is the north–south component and the other side the east–west component. A three-story building is located at the south part of the main building (shaded square). (c) North–south and east–west vertical cross sections. Elevations are relative to the ground level (0 m) of the building. In all panels, triangles show the locations of receivers. The details of the building are shown in Figure A1. The color version of this figure is available only in the electronic edition.

nearest K-NET station (a strong-motion seismometer: TKY005) is 147.7 cm/s^2 . The K-NET station is $\sim 2.5 \text{ km}$ south from the building. The building was built in 1991, and Table 1 shows the earthquakes recorded by TKY005 since 1996. No strong-motion records around the building are available before 1996. Based on Table 1, the Tohoku-Oki earthquake was the largest earthquake for this building according to the peak ground acceleration (PGA). The building is an “H” shape reinforced concrete structure, and the height of the central part (east–west) is 47 m and that of the wing parts is 25 m (Fig. 2). A three-story building is located at the south part of the main building (the shaded square in Fig. 2b). Figure A1 shows details of the main structural elements. We define the component parallel to the 79.4 m side is north–south and perpendicular to the east–west component.

Table 1

Earthquakes Recorded by the K-NET Station, TKY005, since 1996 (peak ground acceleration $> 50 \text{ cm/s}^2$)

Date (yyyy/mm/dd)	Distance (km)	Magnitude	PGA (cm/s^2)
1996/08/09	41	4.6	60.2
2005/07/23	65	6.0	75.7
2007/07/12	27	4.2	60.2
2008/08/08	12	4.6	51.5
2011/03/11	416	9.0	147.7
2011/03/15	70	6.4	71.4
2012/01/28	41	5.4	54.5

We distributed six one-component velocity meters (VSE-15D) at the east edge of the building (the triangles in Fig. 2) to record seismic motion. Because of the receivers, we observed earthquakes in different time intervals for the north–south and east–west components. We recorded data in three time periods: 2 months before (before Tohoku), 6 months after (after Tohoku), and 16 months after (after + 1 yr) the Tohoku-Oki earthquake (Table 2). We did not record the motion generated by the mainshock itself. During the year between the second and third observations (after Tohoku and after + 1 yr, respectively), people maintained the building (e.g., filling small cracks with surface sealing). All fixes were very minor and not structural repairs. We did not find visible damages except the small cracks inside and outside the building. The receiver locations do not change over all observations. Although the surveys are continuously recording during these time periods and ambient noise is also useful for monitoring the building (Prieto *et al.*, 2010; Nakata and Snieder, 2014), we focus on earthquake records here. We observed in total more than 300 earthquakes over the time intervals (Fig. 1 and Table 2).

Figure 3 shows an example of earthquake records in the time and frequency domains. The earthquakes occurred on 5 September 2011 at about 150 km east from the building at 23.9 km depth (141.21° E , 35.382° N). The magnitude of the earthquake is 3.7. The average interstory drift caused by this earthquake is 0.00128%, which is computed as the maximum difference of displacements between the ninth and first floors divide by the distance of these sensors (Todorovska, 2009b). Generally, the fundamental mode (around 2 Hz) is prominent in earthquake records, and waveforms in the time domain are monochromatic. After applying deconvolution interferometry (equation 2) to the waveforms in Figure 3, we obtain deconvolved wavefields shown in Figure 4. At times close to 0 s, traveling waves are reconstructed and then the fundamental mode is dominant in later times caused by stronger attenuation in higher modes. Because the earthquake is not very strong, we obtain some traveling-wave energy in the negative time similar to figure 11 of Nakata *et al.* (2013) (due to other vibrations in the building [Nakata and Snieder, 2014]). Here, we focus on the signals in the positive time. Because we change the boundary condition by computing deconvolution, the waveforms at floor 1 become a band-limited delta function (see equation 2 with $z = 0$). The

Table 2

Observation Periods and Number of Earthquakes (in Parentheses)

	Before Tohoku	After Tohoku	After + 1 Yr
North–south	2010/12/20 to 2011/01/01 (48)	2011/08/13 to 2011/09/02 (86)	2012/07/02 to 2012/07/13 (40)
East–west	2011/01/01 to 2011/01/10 (15)	2011/09/02 to 2011/09/16 (106)	2011/07/13 to 2011/07/23 (32)

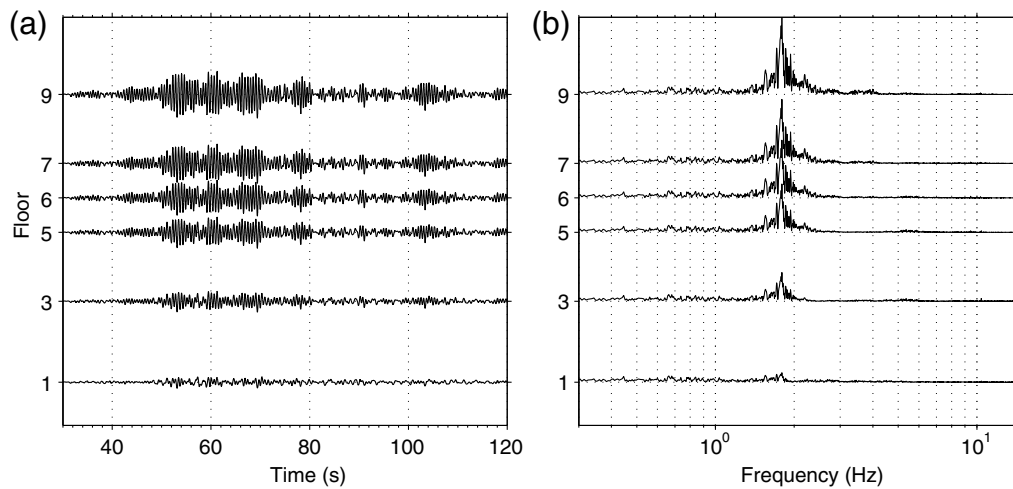


Figure 3. Example of earthquake records observed by the east–west component in the (a) time and (b) frequency domains. The earthquake occurred on 5 September 2011. The time 0 s in (a) represents the origin time of the earthquake. Traces are aligned with the elevation of each floor, and zero amplitudes at each floor are illustrated by the horizontal dashed lines.

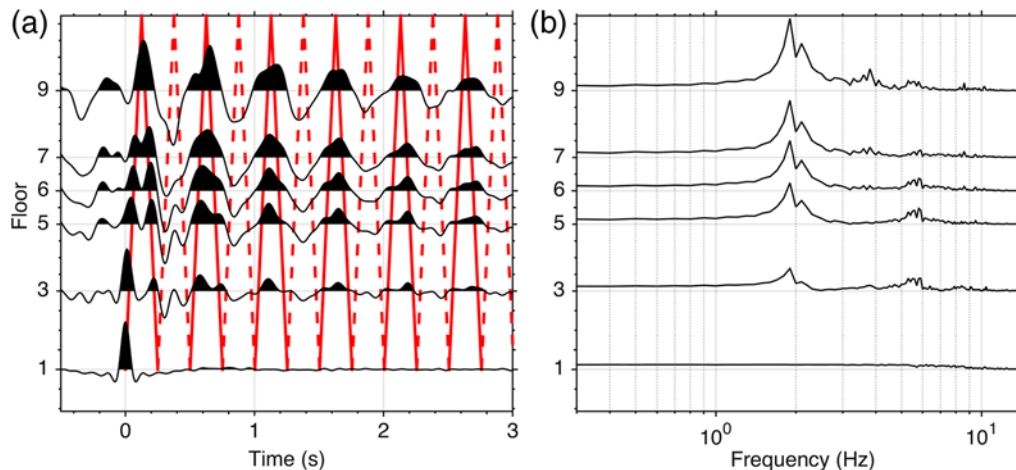


Figure 4. (a) Deconvolved waveforms and (b) their power spectra of the earthquake used in Figure 3. Traces are aligned with the elevation of each floor, and zero amplitudes at each floor are illustrated by the horizontal dashed lines. In (a), we apply a band-pass filter (0.8–20 Hz) to the waveforms. The straight lines in panel (a) represent the arrival times of the wave with the velocity 340 m/s estimated by least-squares fitting of traveling times of the first upgoing deconvolved wavefields. The solid and dashed lines indicate positive and negative polarities based on equation (2). The color version of this figure is available only in the electronic edition.

frequency of the fundamental model ($D(z, 0, \omega)$ in equation 2; Fig. 4b) is higher than $u(z, \omega)$ (Fig. 3b); these differences are related to the wave propagation outside the building and soil–structure interaction.

From the traveling waves in Figure 4a, we can estimate the velocities of the wave propagating inside the building (Snieder and Şafak, 2006). In this study, we estimate velocities from travel times of the first-upgoing deconvolved wavefields with least-squares fitting (Nakata *et al.*, 2013). The velocity of the traveling waves extracted from the earthquake in Figure 3 is 340 m/s (the straight lines in Fig. 4a). For computing the power spectra of the deconvolved waves, we use wavefields in -0.5 to 5 s because the wavefields in later times strongly attenuate and the signal-to-noise ratio is

small. Because the shorter-time interval is used for Figure 4b than Figure 3b, the frequency resolution in deconvolved wavefields is lower but enough to estimate accurate frequencies of normal modes. In the next section, we apply deconvolution interferometry to all earthquakes to estimate damage caused by the Tohoku-Oki earthquake.

Damage of the Tohoku-Oki Earthquake Estimated by Deconvolution

In Figure 5, we estimate velocities of deconvolved wavefields from each earthquake with the method mentioned in the previous section. Compared with before the Tohoku-Oki earthquake, velocities after the mainshock decrease

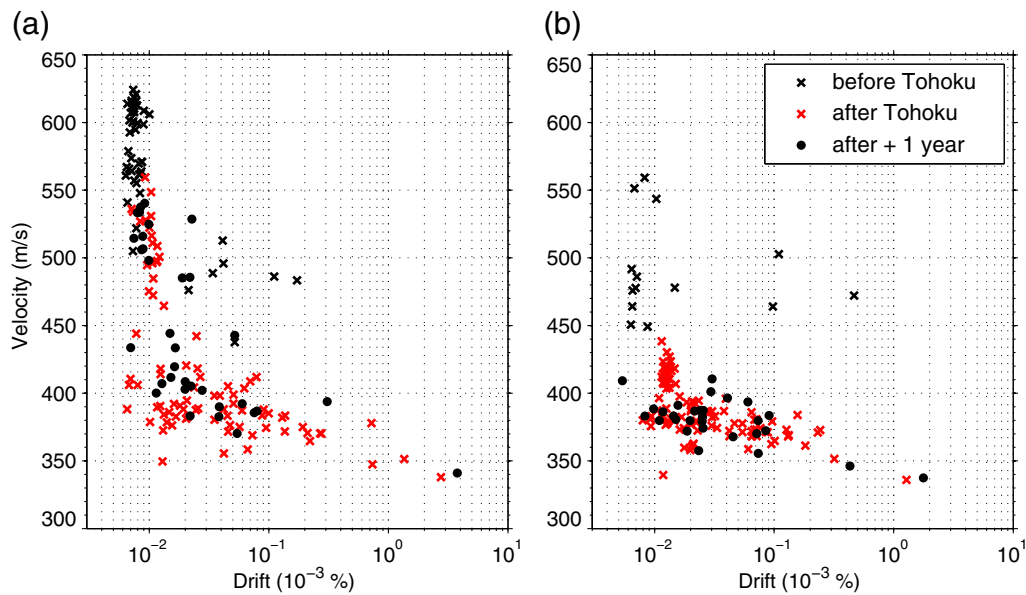


Figure 5. Velocities of traveling waves after deconvolution in the (a) north–south and (b) east–west components. The velocities are estimated from the first upgoing deconvolved waveforms with least-squares fitting of the straight line. Each mark shows the velocity of each earthquake. Drift is the maximum difference of displacements between top and bottom receivers divided by the distance of these receivers. The color version of this figure is available only in the electronic edition.

$\sim 20\%$ in both components. We can interpret this reduction as a weakening of the building. We do not find clear patterns of estimated velocities according to the location of earthquakes used, which indicates that this technique is robust for earthquake locations. In Figure 5, we compare the velocities with the average interstory drift. The velocities have a mildly negative correlation with the drifts.

We also estimate frequencies of the fundamental mode of deconvolved wavefields for each earthquake (Fig. 6). To estimate the accurate frequencies, we use a least-squares fitting of a Gaussian curve (Menke, 2012). This fitting overcomes the poor signal-to-noise ratio at some earthquakes. The shapes of distributions of points in Figures 5 and 6 are similar each other. If the assumptions in equation (1) are satisfied and the deconvolved wavefields are perfectly decoupled from the medium outside the building, we hold a linear relationship of $v_0 = 4Hf_0$, in which v_0 and f_0 are the velocity and peak frequency of the fundamental mode, respectively. For example, the peak frequency of the fundamental mode in Figure 4 is 1.9 Hz. Because the distance of the traveling wave is between the receiver at the first floor to the roof (42.24 m), the expected velocity of the fundamental mode is $4 \times 42.24 \times 1.9 = 321$ m/s, which is close to the velocity (340 m/s) we obtained from the traveling waves in Figure 4. The velocities in Figure 5 contain higher frequency information, and thus the shape is slightly different from that in Figure 6.

For a statistical comparison of the fundamental-mode frequencies, we compute means and standard deviations over all earthquakes in each time interval and is shown in Figure 7. Based on Student's t -test (Bulmer, 1979), frequencies significantly decrease after the Tohoku-Oki earthquake in both com-

ponents (probability $> 99\%$). The reduction is slightly larger in the east–west component (20%) than the north–south component (18%). Between the two time periods after the mainshock, the frequency recovers in the east–west component (8% of the reduction), but the increase in the north–south component is not significant. Although we need further investigation to find reasons of this recovery, the maintenance between September 2011 and July 2012 was very minor and we speculate that it did not cause the change in structural response. In addition, people filled small cracks on walls without preference of directions (e.g., north–south or east–west). The building has a different shape in the north–south and east–west directions, and the difference could be related to the different recovery processes in these components.

Comparison of Fundamental-Mode Frequencies between Deconvolution and Observation

We can also estimate the frequencies of the fundamental mode from observed data (e.g., Fig. 3b), which contain responses of the building and the structure along the wavepath. In Figure 7, we also illustrate means and standard deviations of the fundamental-mode frequencies obtained from observed data. As we expected from equations (1) and (2), the frequencies estimated from observation are lower than those from deconvolution because of the change of the boundary condition at the base. Because of the spectral division shown in equation (2), we can cancel some responses of structure outside the building. Even though the observation lines in Figure 7 show statistically significant reduction of frequencies caused by the Tohoku-Oki earthquake similar

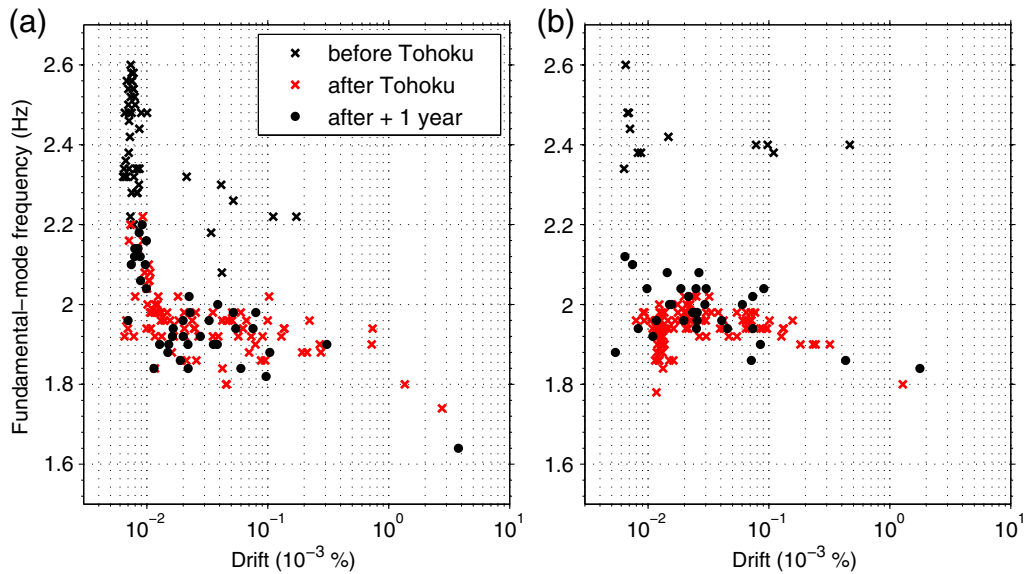


Figure 6. Frequencies of the fundamental mode estimated from deconvolved wavefields in the (a) north–south and (b) east–west components. Power spectra for this estimation are computed from time interval -0.5 to 5 s of deconvolved waveforms with least-squares fitting of a Gaussian curve. Each mark shows the frequency of each earthquake. Drift is the maximum difference of displacements between top and bottom receivers divided by the distance of these receivers. The color version of this figure is available only in the electronic edition.

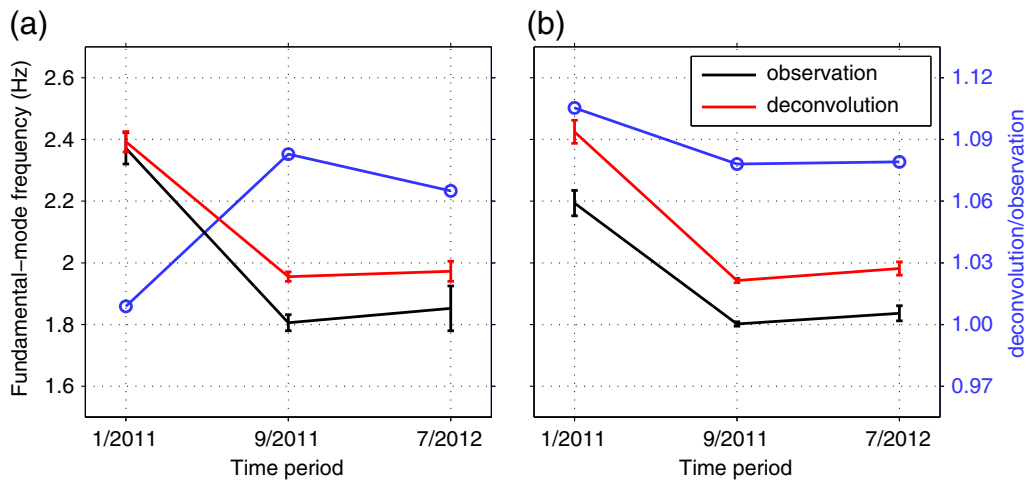


Figure 7. Mean frequencies of the fundamental mode averaged over all earthquakes in each time period computed from observed and deconvolved wavefields in the (a) north–south and (b) east–west components. Error bars show two standard deviations of each mean ($E(f_0) \pm \sigma$). The lines with circles (right axes) indicate the ratio of frequencies between observation and deconvolution at each time interval. The color version of this figure is available only in the electronic edition.

to the deconvolution lines, the amount of reduction compared with deconvolution lines is different. The ratio of mean frequencies (deconvolution/observation, Fig. 7) is useful to qualitatively interpret the locations of the damage cause by the mainshock. Interestingly, we obtain different responses depending on components; the reduction in the frequency for the observation is larger in the north–south component and vice versa in the east–west component. The different responses may be related to the shape of the building and/or anisotropy of the soil under the building.

Figure 8 shows crossplots of the fundamental-mode frequencies obtained from observed and deconvolved wavefields. Dots and crosses above the black line indicate that the frequencies of deconvolution are higher than those of observation. Most of the fundamental-mode frequencies obtained from deconvolved wavefields are higher than those from observed wavefields due to the absence of the response in the deconvolved wavefields. This phenomenon is common for all time intervals in both components. At higher frequencies of each time period in Figure 8a, some data points are

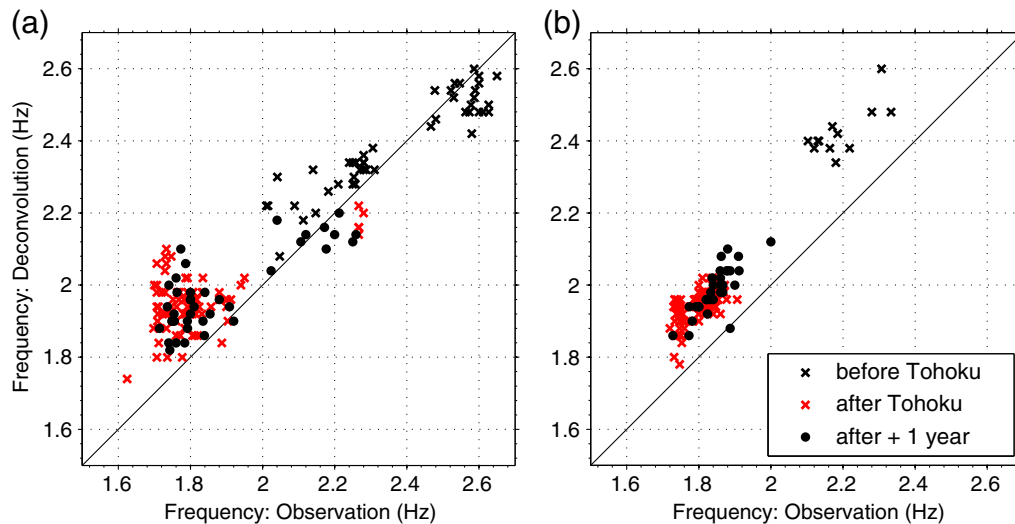


Figure 8. Crossplots of frequencies for the fundamental model estimated from observed and deconvolved wavefields in the (a) north-south and (b) east-west components. Each mark shows the frequency of each earthquake. The color version of this figure is available only in the electronic edition.

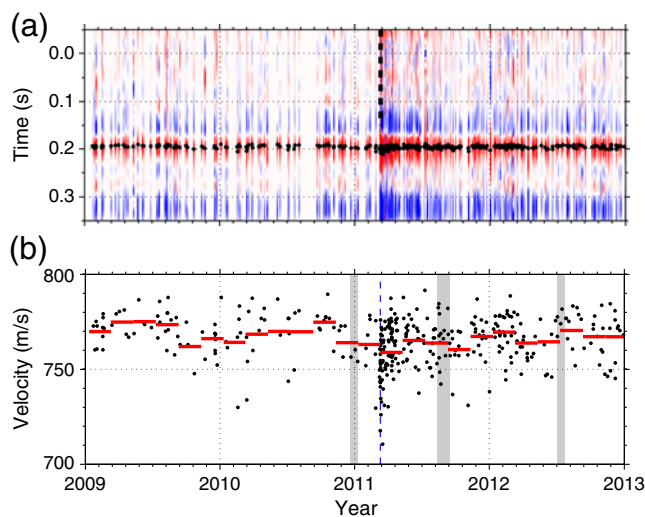


Figure 9. Time-lapse changes in travel times and velocities between 2009 and 2012 at the nearest KiK-net station (TKYH12: 13 km northwest from the building). (a) Arrival times of the propagating waves from the downhole station to the surface station at each earthquake. The background image shows deconvolved waveforms. (b) *S*-wave velocities computed from the travel times at each earthquake (dots). The horizontal bars indicate averaged velocities over all earthquakes occurred in each two months (e.g., from 11 March 2011 to 11 May 2011). The shades show the time periods of observation at the building. The vertical dashed lines in both panels indicate the origin time of the Tohoku-Oki earthquake. The color version of this figure is available only in the electronic edition.

separated from the main cluster of the data. For example, in the before Tohoku data, the main cluster is around 2.2 Hz and the scattered cluster at 2.5 Hz. We need more data to understand this phenomenon and will deploy spatially dense sensors to record building motion.

Nakata and Snieder (2011) estimated the changes in near-surface (~ 100 m) *S*-wave velocities between before and after the Tohoku-Oki earthquake by applying deconvolution interferometry to strong-motion records observed by KiK-net. The velocity reduction they found around the building is $< 1\%$. Figure 9 shows the deconvolved wavefields and estimated velocities at the nearest KiK-net station (TKYH12). The near-surface condition at TKYH12 and the building is similar; a soft-loam layer (5–10 m) is on top of a sand layer. Based on Figure 9, the reduction in near-surface velocities after the Tohoku-Oki earthquake is not large ($< 1\%$), and we cannot explain the velocity reduction in Figure 7, and hence the reduction in Figure 7 is related to the building.

Conclusions

We apply deconvolution interferometry to earthquake data observed inside the building at Tokyo Metropolitan University and obtain reduction in velocities and frequencies of the fundamental mode of the building after the Tohoku-Oki earthquake. The reduction, which partly recovers after 16 months from the mainshock in one component, is about 20%, and we can interpret the reduction as weakening of the building. The reduction is much larger than that at the near-surface structure. By comparing the fundamental-mode frequencies obtained from deconvolved and observed wavefields, we understand that we can cancel some response outside the building and the frequencies of deconvolved waves are always higher than those of observed waves. Although the shape of the building is not the best for seismic interferometry as used for other studies, we demonstrate that we can still use the same technique and obtain useful responses.

Data and Resources

The earthquake catalog was provided by the Japan Meteorological Agency, and strong motion was recorded by the National Research Institute for Earth Science and Disaster Prevention. Figure 1 was produced by using the Generic Mapping Tools (<http://gmt.soest.hawaii.edu>; last accessed July 2014).

Acknowledgments

We thank the Tokyo Metropolitan University for the permission to acquire the seismic data. This study is supported by the Long-Term Safety for Aging Infrastructure Constructions at the Tokyo Metropolitan University. We are grateful to Maria I. Todorovska for her thorough review and useful comments. Nori Nakata thanks the financial support of the George Thompson Fellowship at Stanford University.

References

- Bulmer, M. G. (1979). *Principles of Statistics*, Dover Publications, New York.
- Claerbout, J. F. (1968). Synthesis of a layered medium from its acoustic transmission response, *Geophysics* **33**, no. 2, 264–269.
- Ebrahimian, M., and M. I. Todorovska (2014). Wave propagation in a Timoshenko beam building model, *J. Eng. Mech.* **140**, 04014018.
- Ebrahimian, M., and M. I. Todorovska (2015). Structural system identification of buildings by a wave method based on a nonuniform Timoshenko Beam model, *J. Eng. Mech.* 04015022.
- Kohler, M. D., T. H. Heaton, and S. C. Bradford (2007). Propagating waves in the steel, moment-frame Factor building recorded during earthquakes, *Bull. Seismol. Soc. Am.* **97**, no. 4, 1334–1345.
- Menke, W. (2012). *Geophysical Data Analysis: Discrete Inverse Theory*, Vol. 3, Academic Press, Waltham, Massachusetts.
- Miyazawa, M., R. Snieder, and A. Venkataraman (2008). Application of seismic interferometry to extract *P*- and *S*-wave propagation and observation of shear-wave splitting from noise data at Cold Lake, Alberta, Canada, *Geophysics* **73**, no. 4, D35–D40.
- Nakata, N. (2013). Combination of Hi-net and KiK-net data for deconvolution interferometry, *Bull. Seismol. Soc. Am.* **103**, no. 6, 3073–3082.
- Nakata, N., and R. Snieder (2011). Near-surface weakening in Japan after the 2011 Tohoku-Oki earthquake, *Geophys. Res. Lett.* **38**, L17,302, doi: [10.1029/2011GL048800](https://doi.org/10.1029/2011GL048800).
- Nakata, N., and R. Snieder (2014). Monitoring a building using deconvolution interferometry. II: Ambient-vibration analysis, *Bull. Seismol. Soc. Am.* **104**, no. 1, 204–213, doi: [10.1785/0120130050](https://doi.org/10.1785/0120130050).
- Nakata, N., J. P. Chang, J. F. Lawrence, and P. Boué (2015). Body-wave extraction and tomography at Long Beach, California, with ambient-noise tomography, *J. Geophys. Res.* **120**, 1159–1173, doi: [10.1002/2015JB011870](https://doi.org/10.1002/2015JB011870).
- Nakata, N., R. Snieder, and M. Behm (2014). Body-wave interferometry using regional earthquakes with multidimensional deconvolution after wavefield decomposition at free surface, *Geophys. J. Int.* **199**, 1125–1137.
- Nakata, N., R. Snieder, S. Kuroda, S. Ito, T. Aizawa, and T. Kunimi (2013). Monitoring a building using deconvolution interferometry. I: Earthquake-data analysis, *Bull. Seismol. Soc. Am.* **103**, no. 3, 1662–1678, doi: [10.1785/0120120291](https://doi.org/10.1785/0120120291).
- Pech, A., F. J. S. Sesma, R. Snieder, F. Ignacio-Caballero, A. Rodríguez-Castellanos, and J. C. Ortíz-Alemán (2012). Estimate of shear wave velocity, and its time-lapse change, from seismic data recorded at the SMNH01 station of KiK-net using seismic interferometry, *Soil Dynam. Earthq. Eng.* **39**, 128–137.
- Prieto, G. A., J. F. Lawrence, and G. C. Beroza (2009). Anelastic earth structure from the coherency of the ambient seismic field, *J. Geophys. Res.* **114**, no. B07303, doi: [10.1029/2008JB006067](https://doi.org/10.1029/2008JB006067).
- Prieto, G. A., J. F. Lawrence, A. I. Chung, and M. D. Kohler (2010). Impulse response of civil structures from ambient noise analysis, *Bull. Seismol. Soc. Am.* **100**, no. 5A, 2322–2328.
- Rahmani, M., M. Ebrahimian, and M. I. Todorovska (2015). Wave dispersion in high-rise buildings due to soil-structure interaction, *Earthq. Eng. Struct. Dynam.* **44**, 317–323.
- Ruigrok, E., X. Campman, D. Draganov, and K. Wapenaar (2010). High-resolution lithospheric imaging with seismic interferometry, *Geophys. J. Int.* **183**, 339–357, doi: [10.1111/j.1365-246X.2010.04724.x](https://doi.org/10.1111/j.1365-246X.2010.04724.x).
- Sawazaki, K., H. Sato, H. Nakahara, and T. Nishimura (2009). Time-lapse changes of seismic velocity in the shallow ground caused by strong ground motion shock of the 2000 western-Tottori earthquake, Japan, as revealed from coda deconvolution analysis, *Bull. Seismol. Soc. Am.* **99**, no. 1, 352–366.
- Snieder, R. (2004a). *A Guided Tour of Mathematical Methods for the Physical Sciences*, Cambridge University Press, Cambridge, United Kingdom, 507 pp.
- Snieder, R. (2004b). Extracting the Green’s function from the correlation of coda waves: A derivation based on stationary phase, *Phys. Rev. E* **69**, 046,610.
- Snieder, R., and E. Şafak (2006). Extracting the building response using seismic interferometry: Theory and application to the Millikan Library in Pasadena, California, *Bull. Seismol. Soc. Am.* **96**, no. 2, 586–598.
- Snieder, R., J. Sheiman, and R. Calvert (2006). Equivalence of the virtual-source method and wave-field deconvolution in seismic interferometry, *Phys. Rev. E* **73**, 066,620, doi: [10.1103/PhysRevE.73.066620](https://doi.org/10.1103/PhysRevE.73.066620).
- Todorovska, M. I. (2009a). Seismic interferometry of a soil-structure interaction model with coupled horizontal and rocking response, *Bull. Seismol. Soc. Am.* **99**, no. 2A, 611–625.
- Todorovska, M. I. (2009b). Soil-structure system identification of Millikan Library north–south response during four earthquakes (1970–2002): What caused the observed wandering of the system frequencies? *Bull. Seismol. Soc. Am.* **99**, no. 2A, 626–635.
- Todorovska, M. I., and M. D. Trifunac (2008). Impulse response analysis of the Van Nuys 7-story hotel during 11 earthquakes and earthquake damage detection, *Struct. Control Health Monit.* **15**, 90–116.
- Trifunac, M. D. (1972). Comparisons between ambient and forced vibration experiments, *Earthq. Eng. Struct. Dynam.* **1**, 133–150.
- Trifunac, M. D., S. S. Ivanović, and M. I. Todorovska (2001). Apparent periods of a building. I: Fourier analysis, *J. Struct. Eng.* **127**, no. 5, 517–526.
- Vasconcelos, I., and R. Snieder (2008). Interferometry by deconvolution: Part 2 Theory for elastic waves and application to drill-bit seismic imaging, *Geophysics* **73**, no. 3, S129–S141.
- Wapenaar, K. (2004). Retrieving the elastodynamic Green’s function of an arbitrary inhomogeneous medium by cross correlation, *Phys. Rev. Lett.* **93**, 254,301.
- Wapenaar, K., J. van der Neut, and E. Ruigrok (2008). Passive seismic interferometry by multidimensional deconvolution, *Geophysics* **73**, no. 6, A51–A56.

Appendix

Structural Elements of the Building

Figure A1 shows the detail of the building with structural elements.

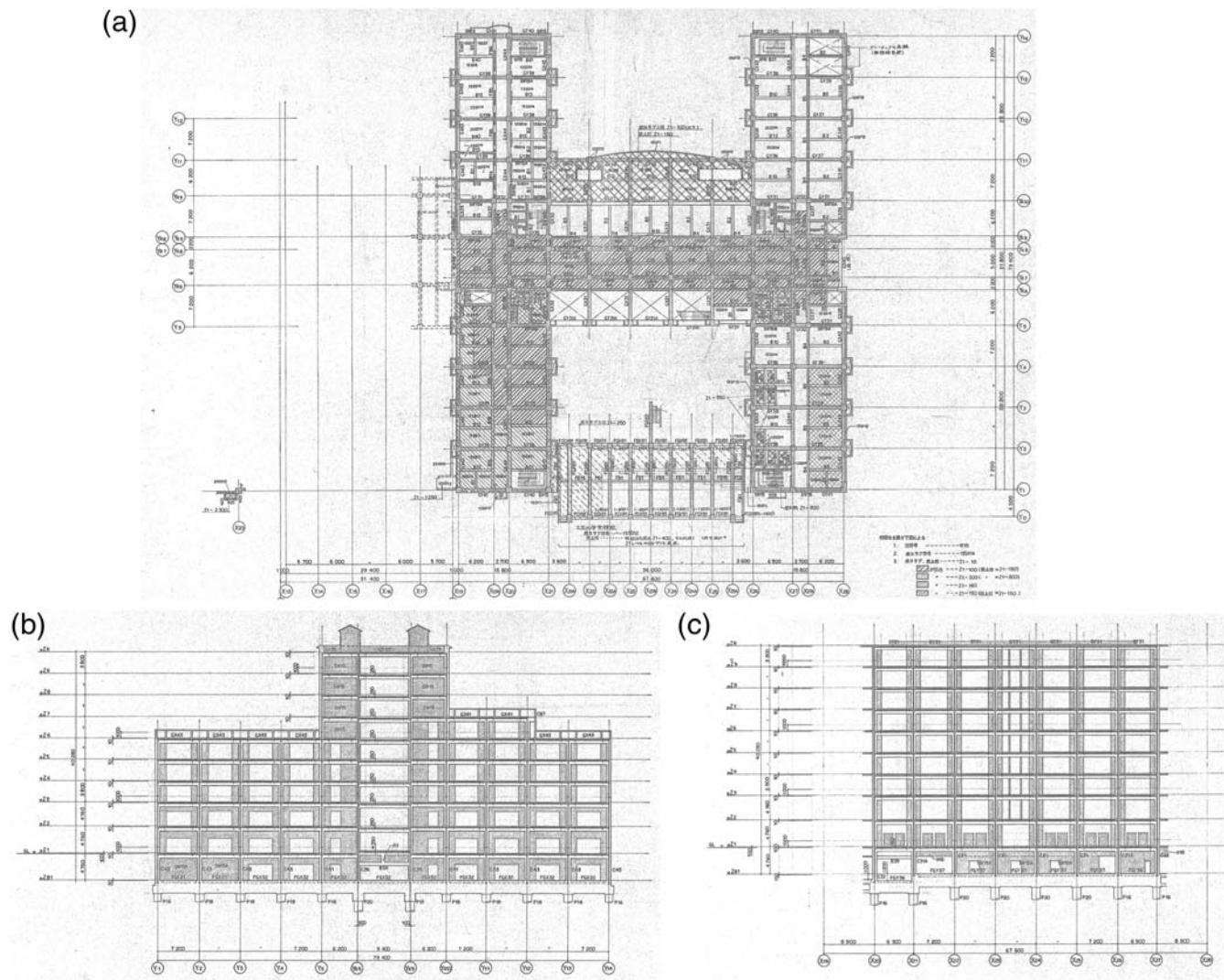


Figure A1. Structural elements of the building in the (a) floor, (b) north-south, and (c) east-west plans.

Stanford University
 Department of Geophysics
 397 Panama Mall
 Stanford, California 94305
 mmakata@stanford.edu
 (N.N.)

Tokyo Metropolitan University
 Department of Civil and Environmental Engineering
 1-1 Minami Oosawa
 Hachioji-shi, Tokyo 192-0397, Japan
 w.27bononchi@gmail.com
 oda@tmu.ac.jp
 (W.T., Y.O.)

Manuscript received 23 July 2014;
 Published Online 18 August 2015